Science R

Cite as: S. S. Shin *et al.*,
10.1126/science.aam6620

Colloidally prepared La-doped $BaSnO_3$ electrodes for efficient, photostable perovskite solar cells

Seong Sik Shin,[1,2] Eun Joo Yeom,[1] Woon Seok Yang,[3] Seyoon Hur,[4] Min Gyu Kim,[5] Jino Im,[1] Jangwon Seo,[1] Jun Hong Noh,[1,6]* Sang Il Seok[1,3]*

[1]Division of Advanced Materials, Korea Research Institute of Chemical Technology, 141 Gajeong-Ro, Yuseong-Gu, Daejeon 34114, Republic of Korea. [2]Massachusetts Institute of Technology, 77 Massachusetts Avenue, Cambridge, MA 02139, USA. [3]Perovtronics Research Center, School of Energy and Chemical Engineering, Ulsan N Institute of Science and Technology, 50 UNIST-gil, Eonyang-eup, Ulju-gun, Ulsan 44919, Republic of Korea. [4]Department of Materials Science and Engineering, Seoul National University, Seoul, 151-744, Republic of Korea. [5]Beamline Research Division, Pohang Accelerator Laboratory (PAL), Pohang 790-784, Republic of Korea. [6]Sch Civil, Environmental and Architectural Engineering, Korea University, Seoul 136-713, Republic of Korea.

***Corresponding author. E-mail: seoksi@unist.ac.kr (S.I.S.); jhnoh@krict.re.kr (J.H.N.)**

Perovskite solar cells (PSCs) exceeding a power conversion efficiency (PCE) of 20% have mainly been demonstrated by using mesoporous titanium dioxide (mp-TiO_2) as an electron-transporting layer. However, TiO_2 can reduce the stability of PSCs under illumination (including ultraviolet light). Lanthan (La)–doped $BaSnO_3$ (LBSO) perovskite would be an ideal replacement given its electron mobility and electronic structure, but LBSO cannot be synthesized as well-dispersible fine particles or crystallized below 500°C. We report a superoxide colloidal solution route for preparing an LBSO electrode under v mild conditions (below 300°C). The PSCs fabricated with LBSO and methylammonium lead iodide ($MAPbI_3$) show a steady-state power conversion efficiency of 21.2%, versus 19.7% for a mp-TiO_2 devic The LBSO-based PSCs could retain 93% of its initial performance after 1000 hours of full Sun illumination.

Fully solidified perovskite solar cells (PSCs) emerged (*1*, *2*) ... several factors, including the instability of the per

a compact, crystalline LBSO thin film below at least 500°C is to coat a desired LBSO colloidal solution that includes well-dispersed precrystalline LBSO perovskite nanoparticles (NPs) onto the substrate. Introducing amorphous precursors containing peroxo groups could reduce the crystalline temperature to 900°C; the amorphous precursors are prepared by mixing aqueous barium chloride and tin chloride solutions with a solution of hydrogen peroxide and NH_3 in water (*28*, *29*). However, the temperature is still too high to fabricate optoelectric devices on a glass substrate. Recently, Huang *et al.* reported a peroxo-precursor synthesis method for mp-BSO at 300°C (*30*). However, these methods could not create a colloidal solution to fabricate the compact BSO perovskite film. Thus, the development of a mass-producible and completely dispersed precursor colloidal solution for producing BSO thin films is a challenging issue for obtaining efficient and photostable PSCs.

We first demonstrate a crystalline superoxide-molecular cluster (CSMC) colloidal solution containing well-dispersed CSMC NPs in 2-methoxyethanol (2ME) that was prepared by the reaction of $BaCl_2$, $SnCl_2$, $La(NO_3)_3$, and H_2O_2 in an NH_4OH aqueous solution at 50°C. We determined that the crystalline LBSO perovskite phase developed below 300°C from CSMC via an intermediate peroxo-complex by using extended x-ray absorption fine structure (EXAFS) analysis and density functional theory (DFT). The compact and uni-

loidal solution is highly transparent because individu
crete NPs (versus aggregates) form by a self-conder
reaction in the H_2O_2-assisted process. Figure 1B show
diffraction (XRD) patterns, measured in air, of t
prepared and annealed powders. The spectrum for t
prepared powder obtained via the CSMC route co
crystalline XRD peaks, whereas the conventional ro
RT) produces an amorphous powder (Fig. 1B).

The crystalline white powder was successfully con
into a pure perovskite BSO phase by annealing for 30
200°C, which requires a much shorter time and lowe
perature than a conventional route such as a solid-st
action and sol-gel process for the pure BSO perovskite
(*32*). By contrast, the amorphous powder produced
did not convert to the perovskite phase even at a
higher temperature (500°C). Thus, the initial crys
phase in the as-prepared powder plays a key role
formation of the BSO perovskite phase at 200°C. Th
pattern of the as-prepared powder shown in Fig. 1
cates that the initial crystalline phase is not an idea
BSO perovskite phase. Infrared (IR) spectroscopic a
was performed to identify the constituents in t
prepared crystalline powders. Figure 1C shows F
transform (FT) infrared (IR) spectra of the as-pr
powders synthesized at 50°C and RT. The amorphou
der synthesized at RT shows stretching frequencies

loidal solution is shown in Fig. 1D. In the precipitates of $Sn(OOH)_x(OH)_{4-x}$ formed from H_2O_2 and NH_4OH mixture in aqueous solution, the value of x will increase with increasing amount of H_2O_2 (*33*). The decomposition of H_2O_2 is affected by various environmental conditions such as heat, catalysis, concentration of H_2O_2, and pH (*37*). As shown in Fig. 1D, the formation of superoxide (SnO-OSn) will be more favorable at a higher x value and at a mild temperature below 90°C via the condensation reaction between –OOH ions. According to previous reports (*37*), the decomposition of H_2O_2 was limited below 30°C at pH 10 to 11, whereas the increase in temperature from 30° to 40°C accelerated the decomposition rate of H_2O_2 up to 3.3-fold at pH 10 to 11. Indeed, we observed that the crystalline superoxide complex appears at solution temperatures between 40° and 70°C (fig. S4A) (*31*), whereas reaction temperatures above 90°C decrease crystallinity (fig. S4A) (*31*). Furthermore, the crystalline phase is formed only at H_2O_2 concentrations above 15% (fig. S4B) (*31*). Under these specific conditions (50°C and 30%), CSMC can be rapidly formed even within 10 min (fig. S4C) (*31*). An adequate temperature and high concentration of H_2O_2 accelerate the formation of superoxide during the reaction that then forms the CSMC. The superoxo groups at surface of CSMC NPs tend to efficiently repel each other via surface charge, which lead to the stable colloidal solution. However, the CSMC phase formed at 90°C does not create

shared Sn-(O)-Sn distributions for the BSO perovskit
tal structure, respectively, revealing that the as-pr
white powder was effectively converted to the pure
skite phase during the in situ experiment at 200°C.
the formation of a superoxide molecular cluster with
ovskite frame can facilitate the synthesis of well-dis
perovskite BSO NPs, even below 500°C.

On the basis of the XRD, IR, and temperature-dep
RDF results, we performed a first-principles calculati
ing DFT to elucidate the origin of the phase evolu
BSO perovskite below 200°C (crystal structures are
in Fig. 2B). The CSMC has structural deformations
cubic symmetry because the octahedral consisting of
six O_2^- molecules maintain their local geometries bu
randomly distributed orientations. This long-range–o
single cluster consisting of Ba^{2+} cations and the hexa
oxostannate anion, $[Sn(O\text{-}O)_6]^{2-}$, in the as-prepared p
initially formed cross-linked Sn-[O-O]-Sn octahedra w
removal of O_2 during heating; the higher temperatu
motes long-range–ordered development of corner-
Sn-(O)-Sn octahedra by way of O_2 removal, finally re
the pure cubic BSO perovskite structure. We hypoth
that the formation of the long-range–ordered single
as a precursor requires lower energy and presents a
pathway to the thermodynamically stable cubic per
BSO phase, as compared to starting from the amo

As shown in the *J-V* curves, the LBSO cell exhibited an open-circuit voltage (V_{oc}) of 1.12 V, a short-circuit current density (J_{sc}) of 23.4 mA/cm^2, and a fill factor (*FF*) of 81.3%, giving an overall PCE of 21.3%, whereas the control device showed an overall PCE of 19.6% with a V_{oc} of 1.07 V, a J_{sc} of 23.3 mA/cm^2, and a *FF* of 78.6%. The superior performance of the LBSO PSC is mainly attributed to a higher V_{oc} and *FF*, which are associated with beneficial effects such as a higher conduction band minimum and electron density of LBSO, and reduced carrier recombination compared to mp-TiO_2. Because the PSCs using LBSO as the ETL exhibited a large hysteresis in their *J-V* curves with reverse and forward sweeps (fig. S7) (*31*), the stabilized PCEs were estimated to determine the real power output of the device by measuring the steady-state photocurrent with an applied voltage at the maximum power point under simulated solar illumination (100 mW cm^{-2}, AM 1.5G). The LBSO PSC showed a stabilized power output of 21.2% near the maximum power point (0.96 V), which closely matched the values extracted from the *J-V* curve with a reverse sweep (Fig. 3B, inset), whereas the TiO_2-based device showed a stabilized PCE of 19.7%. The reverse-sweep *J-V* curve for the LBSO PSC is notable, although the underestimated forward-sweep *J-V* curve requires further study. Figure S8 shows the time-correlated single-photon counting (TCSPC) results for perovskite samples on different substrates (glass, TiO_2, and LBSO) to investigate

tostability under light illumination, including UV marked UV-induced degradation in PCEs for TiO_2 PSCs presents a serious problem (*14*, *15*, *18*) for their cal use under natural sunlight. So far, PSCs claiming stability have been tested with white light–emitting di UV-filtered solar simulators (*40*, *41*). We conducted a soaking experiment by monitoring the *J-V* charact under AM 1.5G illumination with a xenon or metal lamp, including UV radiation to estimate the photost under 1-sun illumination for the LBSO- and TiO_2- PSCs. Figure 4A shows the monitored PCEs of the un sulated FTO/LBSO/$MAPbI_3$/PTAA/Au FTO/TiO_2/$MAPbI_3$/PTAA/Au devices in a nitroge chamber with a constant device temperature of 25° constant AM 1.5G illumination with a xenon lamp LBSO cell showed a greater resistance against photo dation than the TiO_2 cell; the latter showed an abru crease in PCE upon initial illumination.

However, a cell architecture that includes organi transport materials (HTMs), such as PTAA or OMeTAD, is inappropriate for estimating the influenc type materials on the photostability for long-term urements (~1000 hours) because organic HTMs can d the PV performance by morphological deformation, diffusion, movable additives, and so forth. To exclu influence of organic HTMs on the photostability te

(2009). doi:10.1021/ja809598r Medline
4. M. Saliba, T. Matsui, K. Domanski, J.-Y. Seo, A. Ummadisingu, S. M. Zakeeruddin, J.-P. Correa-Baena, W. R. Tress, A. Abate, A. Hagfeldt, M. Grätzel, Incorporation of rubidium cations into perovskite solar cells improves photovoltaic performance. *Science* **354**, 206–209 (2016). doi:10.1126/science.aah5557 Medline
5. W. S. Yang, J. H. Noh, N. J. Jeon, Y. C. Kim, S. Ryu, J. Seo, S. I. Seok, SOLAR CELLS. High-performance photovoltaic perovskite layers fabricated through intramolecular exchange. *Science* **348**, 1234–1237 (2015). doi:10.1126/science.aaa9272 Medline
6. J. H. Heo, S. H. Im, J. H. Noh, T. N. Mandal, C.-S. Lim, J. A. Chang, Y. H. Lee, H. Kim, A. Sarkar, M. K. Nazeeruddin, M. Grätzel, S. I. Seok, Efficient inorganic-organic hybrid heterojunction solar cells containing perovskite compound and polymeric hole conductors. *Nat. Photonics* **7**, 486–491 (2013). doi:10.1038/nphoton.2013.80
7. M. Liu, M. B. Johnston, H. J. Snaith, Efficient planar heterojunction perovskite solar cells by vapour deposition. *Nature* **501**, 395–398 (2013). doi:10.1038/nature12509 Medline
8. O. Malinkiewicz, A. Yella, Y. H. Lee, G. M. Espallargas, M. Graetzel, M. K. Nazeeruddin, H. J. Bolink, Perovskite solar cells employing organic charge-transport layers. *Nat. Photonics* **8**, 128–132 (2014). doi:10.1038/nphoton.2013.341
9. D.-Y. Son, J.-H. Im, H.-S. Kim, N.-G. Park, 11% efficient perovskite solar cell based on ZnO nanorods: An effective charge collection system. *J. Phys. Chem. C* **118**, 16567–16573 (2014). doi:10.1021/jp412407j
10. J. P. Correa-Baena, L. Steier, W. Tress, M. Saliba, S. Neutzner, T. Matsui, F. Giordano, T. J. Jacobsson, A. R. Srimath Kandada, S. M. Zakeeruddin, Highly efficient planar perovskite solar cells through band alignment engineering. *Energy Environ. Sci.* **8**, 2928–2934 (2015). doi:10.1039/C5EE02608C
11. S. S. Shin, W. S. Yang, J. H. Noh, J. H. Suk, N. J. Jeon, J. H. Park, J. S. Kim, W. M. Seong, S. I. Seok, High-performance flexible perovskite solar cells exploiting Zn_2SnO_4 prepared in solution below 100 °C. *Nat. Commun.* **6**, 7410 (2015).
Santhala, S. I. Watanabe, D. J. Hollman, N. Noel, A. Sepe, U. Wiesner, H. J. Snaith, U. Steiner, Performance and stability enhancement sensitized and perovskite solar cells by Al doping of TiO_2. *Adv. Funct.* 6046–6055 (2014). doi:10.1002/adfm.201401658
21. D. O. Scanlon, Defect engineering of $BaSnO_3$ for high-performance tra conducting oxide applications. *Phys. Rev. B* **87**, 161201 doi:10.1103/PhysRevB.87.161201
22. Y. M. Kim, C. Park, U. Kim, C. Ju, K. Char, High-mobility $BaSnO_3$ transistor with HfO_2 gate insulator. *Appl. Phys. Express* **9**, 01120 doi:10.7567/APEX.9.011201
23. J. Cerdà, J. Arbiol, G. Dezanneau, R. Diaz, J. Morante, Perovskite-typ powders for high temperature gas sensor applications. *Sens. Actuators* **84**, 21–25 (2002). doi:10.1016/S0925-4005(02)00005-9
24. H. J. Kim, U. Kim, H. M. Kim, T. H. Kim, H. S. Mun, B.-G. Jeon, K. T. Ho Lee, C. Ju, K. H. Kim, K. Char, High mobility in a stable transparent p oxide. *Appl. Phys. Express* **5**, 061102 (2012). doi:10.1143/APEX.5.06110
25. W. Zhang, J. Tang, J. Ye, Photoluminescence and photocatalytic pro $SrSnO_3$ perovskite. *Chem. Phys. Lett.* **418**, 174–178 doi:10.1016/j.cplett.2005.10.122
26. W. Wang, S. Liang, K. Ding, J. Bi, J. C. Yu, P. K. Wong, L. Wu, M hydrothermal synthesis of $MSnO_3$ (M^{2+}= Ca^{2+}, Sr^{2+}, Ba^{2+}): Effect of M^{2+} structure and photocatalytic properties. *J. Mater. Sci.* **49**, 1893–190 doi:10.1007/s10853-013-7880-x
27. P. Wadekar, J. Alaria, M. O'Sullivan, N. Flack, T. Manning, L. Phillips, K. D Lozano, S. Lucas, J. Claridge, M. J. Rosseinsky, Improved electrical m highly epitaxial La: BaSnO3 films on $SmScO_3$ (110) substrates. *Appl. P* **105**, 052104 (2014). doi:10.1063/1.4891816
28. G. Pfaff, Wet chemical synthesis of $BaSnO_3$ and Ba_2SnO_4 powders. *J. Eu Soc.* **12**, 159–164 (1993). doi:10.1016/0955-2219(93)90137-G
29. S. S. Shin, J. S. Kim, J. H. Suk, K. D. Lee, D. W. Kim, J. H. Park, I. S. C Hong, J. Y. Kim, Improved quantum efficiency of highly efficient p $BaSnO_3$-based dye-sensitized solar cells. *ACS Nano* **7**, 1027–103

properties of La-doped $BaSnO_3$ thin films grown by PLD. *J. Phys. Chem. Solids* **76**, 64–69 (2015). doi:10.1016/j.jpcs.2014.07.024

40. M. Saliba, T. Matsui, J.-Y. Seo, K. Domanski, J.-P. Correa-Baena, M. K. Nazeeruddin, S. M. Zakeeruddin, W. Tress, A. Abate, A. Hagfeldt, M. Grätzel, Cesium-containing triple cation perovskite solar cells: Improved stability, reproducibility and high efficiency. *Energy Environ. Sci.* **9**, 1989–1997 (2016). doi:10.1039/C5EE03874J Medline
41. W. Chen, Y. Wu, Y. Yue, J. Liu, W. Zhang, X. Yang, H. Chen, E. Bi, I. Ashraful, M. Grätzel, L. Han, Efficient and stable large-area perovskite solar cells with inorganic charge extraction layers. *Science* **350**, 944–948 (2015). doi:10.1126/science.aad1015 Medline
42. X. Luo, Y. S. Oh, A. Sirenko, P. Gao, T. Tyson, K. Char, S.-W. Cheong, High carrier mobility in transparent $Ba_{1-x}La_xSnO_3$ crystals with a wide band gap. *Appl. Phys. Lett.* **100**, 172112 (2012). doi:10.1063/1.4709415
43. Z. Lebens-Higgins, D. O. Scanlon, H. Paik, S. Sallis, Y. Nie, M. Uchida, N. F. Quackenbush, M. J. Wahila, G. E. Sterbinsky, D. A. Arena, J. C. Woicik, D. G. Schlom, L. F. J. Piper, Direct observation of electrostatically driven band gap renormalization in a degenerate perovskite transparent conducting oxide. *Phys. Rev. Lett.* **116**, 027602 (2016). doi:10.1103/PhysRevLett.116.027602 Medline
44. C. Shan, T. Huang, J. Zhang, M. Han, Y. Li, Z. Hu, J. Chu, Optical and electrical properties of sol–gel derived $Ba_{1-x}La_xSnO_3$ transparent conducting films for potential optoelectronic applications. *J. Phys. Chem. C* **118**, 6994–7001 (2014). doi:10.1021/jp500100a
45. B. Luo, J. Zhang, J. Wang, P. Ran, Structural, electrical and optical properties of lanthanum-doped barium stannate. *Ceram. Int.* **41**, 2668–2672 (2015). doi:10.1016/j.ceramint.2014.10.080
46. A. Nelson, J. Adams, K. Schaffers, Photoemission investigation of the electronic structure of lanthanum–calcium oxoborate. *J. Appl. Phys.* **94**, 7493–7495 (2003). doi:10.1063/1.1627955

ACKNOWLEDGMENTS

This work was supported by Global Frontier R&D Program for Multiscale Energy

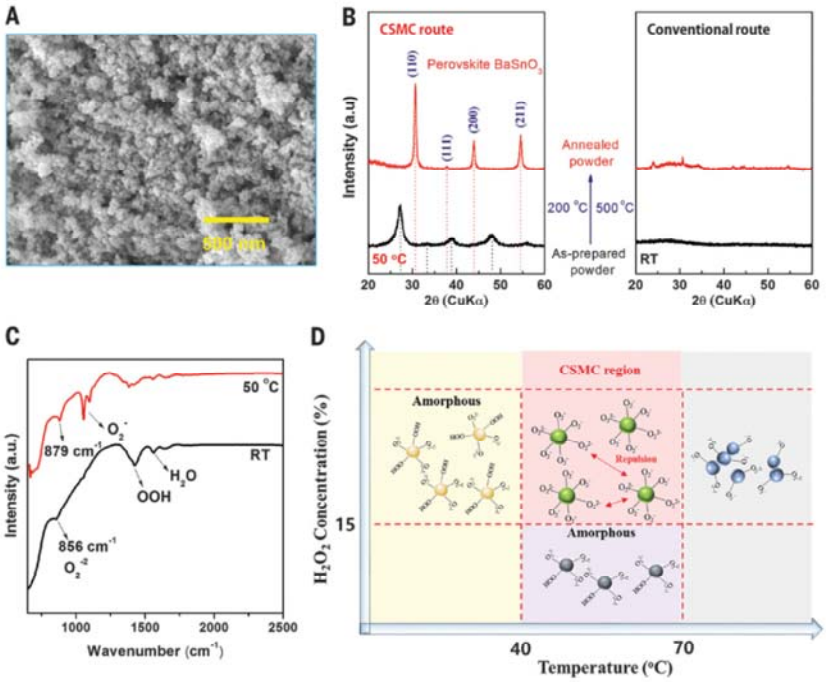

Fig. 1. Synthesis of CSMC BSO. (A) SEM image of the prepared BSO po synthesized at 50°C. (B) spectra of the as-prep powder synthesized at 50°C annealed powder at 200°C fo min (left), and the as-prep powder synthesized at r temperature and annealed 500°C for 1 hour via conventional route (right). FT-IR spectra of the as-prep BSO powder synthesized room temperature and 50°C Schematic illustration of formation map for superoxide precursor coll solution.

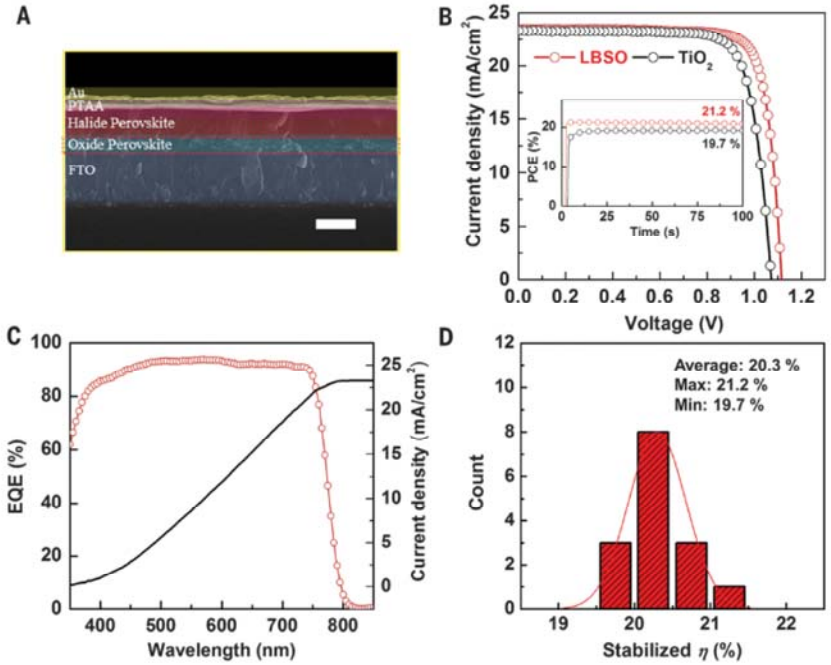

Fig. 3. Photovo
performance of PSCs
Cross-sectional SEM imag
LBSO-based PSCs (scale
500 nm). (B) *J-V* curves,
(inset) stabilized PCEs a
maximum power point (LI
0.96 V; TiO_2: 0.91V) for the b
performing LBSO- and
based PSC. (C) EQE spec
and J_{sc} integrated from the
spectrum of the best-perfor
LBSO-based PSC.
Histograms of PCEs extra
from a photocurrent de
stabilized at the maximum p
point during 100 s for the LB
based PSCs.

Colloidally prepared La-doped $BaSnO_3$ electrodes for efficient, photostable perovskite solar cells

Seong Sik Shin, Eun Joo Yeom, Woon Seok Yang, Seyoon Hur, Min Gyu Kim, Jino Im, Jangwon Seo, Jun Hong Noh and Sang Il Seok

(March 30, 2017)
published online March 30, 2017

Editor's Summary